Some Graphical Interpretations of Melan's Theorem for Shakedown Design

N. Vermaak, M. Boissier, L.Valdevit and R. M. McMeeking

Abstract Bree Interaction Diagrams have long been one of the major visual design guides for employing and evaluating shakedown in engineering applications. These diagrams provide representations of the realms in which elastoplastic behaviors, including shakedown, are found for a material and structure under variable loads. The creation of these diagrams often relies upon some combination of upper or lower bound shakedown theorems and numerical shakedown limit determination techniques. Part of the utility of these diagrams is that, for a given structure and loading conditions, inspecting them is sufficient to determine whether shakedown will occur or not. The diagrams cannot however, give the designer insight into how the conditions for shakedown are met. This chapter presents some graphical interpretations of one of the common methods for shakedown determination: the use of Melan's Lower Bound Theorem. The intent is to provide additional insight for designers regarding how shakedown conditions are satisfied. In this way, additional directions for modifying designs to recover shakedown behavior may also be identified. Revisiting this well-established theorem from a graphical and pedagogical approach, also provides a foundation for interdisciplinary innovation. The particular focus is on simple examples that highlight ways in which Melan's theorem may be applied to shakedown design problems.

N. Vermaak (✉) · M. Boissier
Department of Mechanical Engineering and Mechanics, Lehigh University,
Bethlehem, PA 18015, USA
e-mail: vermaak@lehigh.edu

M. Boissier
e-mail: mathilde.boissier@polytechnique.org

L. Valdevit
Department of Mechanical and Aerospace Engineering, University of California,
Irvine, CA 92697, USA
e-mail: valdevit@uci.edu

R.M. McMeeking
Mechanical Engineering Department, University of California,
Santa Barbara, CA 93106, USA
e-mail: rmcm@engineering.ucsb.edu

O. Barrera et al. (eds.), *Advances in Direct Methods for Materials and Structures*, DOI 10.1007/978-3-319-59810-9_11

1 Introduction

While shakedown concepts, limit theorems, and numerical methods have been developed since the 1920s and 1930s [1–5], their widespread acceptance and application in engineering design communities remains limited [5]. Some of the factors that would promote more widespread use of shakedown concepts and limit theorems include improving awareness through educational materials, more experimental validation efforts, and enhanced communication of shakedown benefits to different design communities. This chapter presents graphical interpretations of shakedown concepts with the intent to provide additional insight and understanding while complementing existing graphical shakedown design tools.

Within the context of plastic design under variable loads, shakedown limit theorems have been used in applications ranging from: vessels for demilitarization of munitions [6], tribology [7], multilayer semiconductor devices [8], pavement design [9, 10], shape memory alloy components [11–13], to nuclear pressure vessels [5]. The theorems delineate the boundaries between reliable and inadmissible behaviors [14–17] (see top of Fig. 1). The theorems often replace traditional yield-limited assessments of structural integrity and can be used in the design process to evaluate a structure's response to unanticipated loads. The operational space is extended by allowing *shakedown* to occur, whereby stresses locally exceed the yield strength of a material in the first few cycles of load and thereafter, fully elastic response is recovered.

More generally, the range of possible structural responses is often illustrated through the use of a Bree Interaction Diagram, which indicates combinations of loads that lead to various material and structural behaviors. Figure 1 illustrates the classic Bree diagram for a thin-walled cylinder (with a radius, R and thickness, t), subjected to a fixed internal pressure and a cyclic radial temperature difference [14]. The ordinate is $\Delta \mathrm{T}/\Delta \mathrm{T}_o$ where $\Delta \mathrm{T}_o$ is the temperature difference required for yield initiation (σ_Y) in the absence of a mechanical load $\left(\Delta T_o = 2(1-\nu)\sigma_Y/E\alpha\right)$; the abscissa is P/P_o with P_o being the pressure that causes yielding in the absence of a temperature gradient $\left(\sigma_Y = P_o R/t\right)$. E, α, ν are the material Young's modulus, coefficient of thermal expansion, and Poisson's ratio, respectively. The elastic domain is defined by $\mathrm{P}/\mathrm{P}_o + \Delta T/\Delta T_o < 1$. At one extreme, wherein $\mathrm{P}/\mathrm{P}_o > 1$, *plastic collapse* occurs on the first load cycle, i.e. the thin wall experiences complete yielding. For intermediate combinations of P and ΔT, one of three behaviors is obtained (Fig. 1) [18]. (i) In the *shakedown* regime, localized plastic deformation that occurs in the early stages of cycling gives rise to residual stresses that stabilize the plastic response. Purely elastic behavior results during any further loading cycles. (ii) *Alternating plasticity* occurs by loading beyond the shakedown limit. Here the plastic strain increment obtained during the first half of each loading cycle is balanced by a plastic strain increment of equal magnitude but opposite sign during the second half of the loading cycle. No net strain accrues during each cycle but the structure ultimately fails by low-cycle fatigue. (iii) *Ratchetting* refers to the condition in which a net increment of plastic strain accumulates during each cycle, eventually causing rupture.

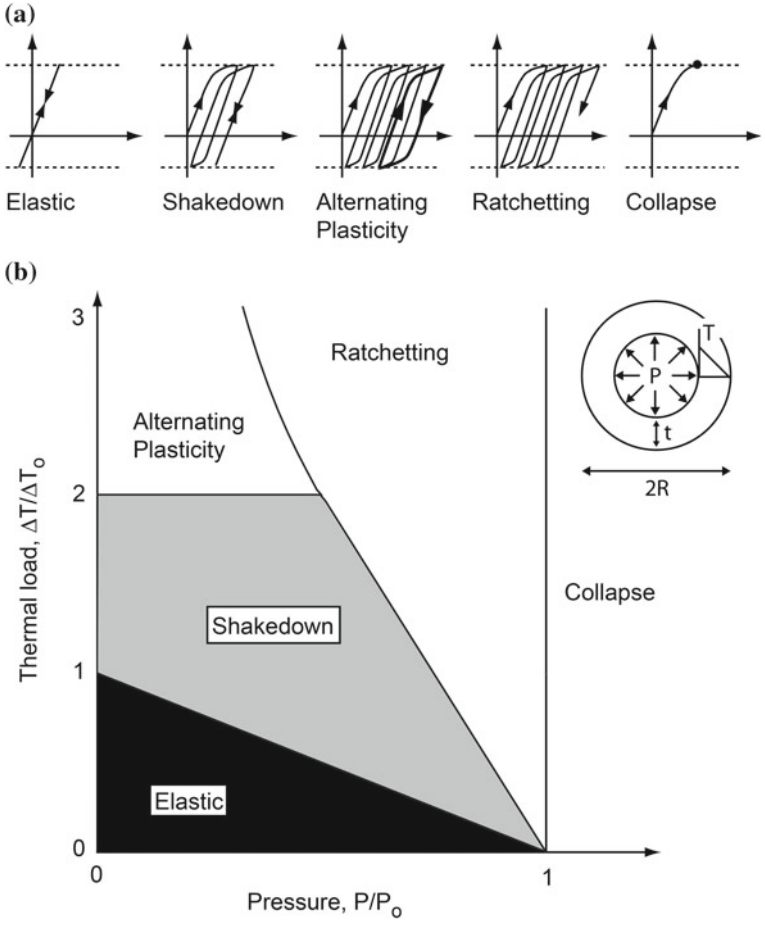

Fig. 1 **a** Prototypical stress-strain behaviors for an elastic-plastic material in the classic Bree problem and **b** the corresponding analytic Bree diagram. A cylindrical vessel is subject to constant internal pressure and a cyclic thermal gradient through the wall thickness

The creation of these diagrams often relies upon some combination of upper or lower bound shakedown theorems and numerical shakedown limit determination techniques. The utility of interaction diagrams such as Fig. 1 is immediately apparent; for an engineering application, designers may easily assess the benefits of allowing shakedown to occur. The interaction diagrams cannot however, give the designer insight into how the conditions for shakedown are met. This chapter presents some graphical interpretations of one of the common methods for shakedown determination: the use of *Melan's Lower Bound Theorem* under small deformation theory assumptions (from Koiter [19]):

> If any time-independent distribution of residual stresses, $\bar{\boldsymbol{\rho}}_{ij}$, can be found such that the sum of these residual stresses and the "elastic" stresses, σ^e_{ij}, is a safe state of stress $\sigma^e_{ij} + \bar{\boldsymbol{\rho}}_{ij} = \sigma^s_{ij}$, *i.e.* a state of stress inside the yield limit, at every point of the body and for all possible load combinations within the prescribed bounds, then the structure will shake down to some time-independent distribution of residual stresses (usually depending on the actual loading program), and the response to subsequent load variations within the prescribed limits will be elastic. On the other hand, shakedown is impossible if no time-independent distribution of residual stresses can be found with the property that the sum of the residual stresses and "elastic" stresses is an allowable state of stress at every point of the body and for all possible load combinations.

In other words, to assure that a structure will shakedown, one has to find a residual stress field, $\boldsymbol{\rho}$, that satisfies the following three conditions: (i) it has to be self-equilibrating, (ii) it has to be time-independent, and (iii) it has to remain within the yield limit when combined with any fictitious "elastic" stress caused by a load combination from the loading domain. This powerful theorem gives a necessary and sufficient condition to determine if a structure will shakedown or not. One of the major advantages of this theorem and this kind of "Direct Method" is that information about the loading path in an arbitrarily complex loading space is not needed. Rigorous bounds and shakedown predictions can be made based on purely elastic solutions or simplified elastoplastic calculations [19–31]. In contrast, the "classical load history approach" follows the incremental or step-by-step evolution of a system and finds the actual residual stress field that would result from the actual loading history that is deterministically known. Direct Methods, which historically developed out of necessity and without access to computational tools, typically take a more mathematical approach to predict shakedown response [5]. It should be noted that "classical incremental or load history approaches" and "direct methods" are not competing methods, but rather complementary as each provides different information and functionality and they often have separate domains of applicability. For example, direct methods avoid cumbersome incremental load-history based calculations and are especially useful when the exact loading history within a domain is unknown. Whereas the load-history based approaches provide the often crucial evolution of local quantities.

Several versions of proofs of Melan's lower bound theorem can be found in the literature [19–21, 32] and many extensions of this theorem have been made to analyze temperature or time-dependent properties, creep, damage, and others [5, 33, 34]. Many ways to implement Melan's theorem to determine shakedown behavior or shakedown limit loads have also been developed; see Weichert and Ponter [5] for a broad historical survey. One way to think about the techniques for lower-bound shakedown determination is by emphasizing "any" in the first part of the limit theorem (*"If **any** time-independent distribution of residual stresses, $\bar{\boldsymbol{\rho}}_{ij}$, can be found..."*). How could one find appropriate residual stress fields? Direct methods exploit the mathematical freedom available by searching for "any" residual stress field that meets the specified shakedown conditions; to do this, direct methods use a variety of procedures from graph theory to optimization [22, 35–43].

In this work, two different direct method implementations of Melan's theorem for shakedown determination are considered. The goal is to illustrate graphically what is mathematically determined when an admissible residual stress field, $\boldsymbol{\rho}$, is sought and the conditions for a structure to shakedown are met. The graphical interpretations also provide a way to understand the role of key parameters and features in the shakedown determination process. Revisiting this well-established theorem from a graphical and pedagogical approach, also provides a foundation for interdisciplinary innovation. In the following, Sect. 2 will present the background and assumptions of the problems analyzed. Sections 3 and 4 present several examples. Discussion of the assumptions and limitations is presented in Sect. 5 and followed by conclusions.

2 Setting of the Problem

Consider an elastic-perfectly-plastic solid, Ω, under small deformation theory assumptions. Its boundary, $\partial\Omega$, characterized by its normal, $\underline{n}$, can be described in parts (Fig. 2): $\partial\Omega_0$ is the part of the boundary on which displacement is imposed, $\partial\Omega_F$ is the part of the boundary on which any traction, F, from the prescribed loading domain, L (Fig. 3), could be applied, and Γ is the part of the boundary that is traction-free. These parts satisfy the conditions:

$$\begin{aligned} &\partial\Omega = \partial\Omega_0 \cup \partial\Omega_F \cup \Gamma, \\ &\partial\Omega_0 \cap \partial\Omega_F = \emptyset, \qquad \partial\Omega_0 \cap \partial\Gamma = \emptyset, \qquad \partial\Omega_F \cap \partial\Gamma = \emptyset. \end{aligned} \tag{1}$$

In the following, a constant scalar yield stress, σ_Y, is considered and a von Mises yield function, f, is adopted. As a result of a load, P, applied to a solid, Ω, on the part $\partial\Omega_F$, two types of stresses will be distinguished: (i) the *actual stresses*, σ^P_{actual}, these are the elastoplastic stresses that would be caused by the load (under the elastic-perfectly-plastic model); (ii) the *fictitious "elastic" stresses*, $\sigma^P_{e,fict}$, these are the stresses that would be caused by the load if the response were purely elastic.

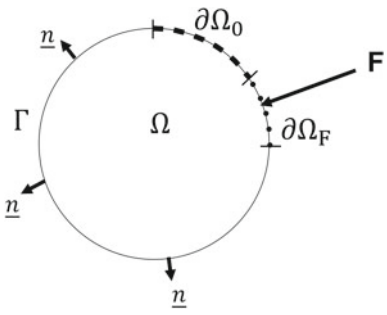

Fig. 2 Schematic of structure and problem parameters

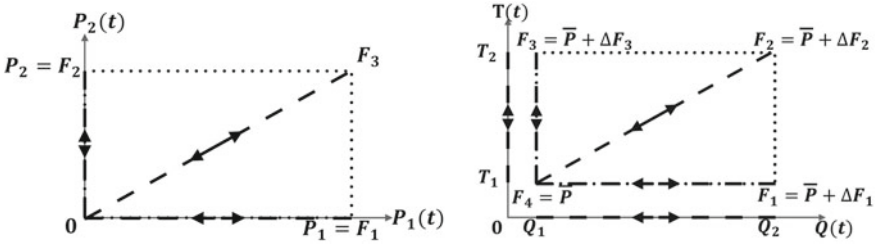

Fig. 3 Loading domains, L

Lastly, the loading domain, L, assumed (Fig. 3) contains every possible loading combination for the loads applied to the solid. By assuming that L is a convex N-dimensional polyhedron [44], it is possible to define the loading corners, F_i, ($i \in [\![1, NC]\!]$ where NC is the number of corners) of the loading domain, and every loading path that connects one corner to another will remain inside the loading domain. Note that all problems considered involve loading by tractions, forces or displacements and no thermal stresses are considered. We therefore keep temperature constant and uniform throughout the examples presented. As a result, two types of loading domains, L, can be considered: only cyclic loads and combined cyclic and constant loads (Fig. 3). For example, at the bottom of Fig. 3, a combined cyclic and constant loading domain is illustrated. It is composed of the loads $Q(t)$ (cycling between Q_1 and Q_2) and $T(t)$ (cycling between T_1 and T_2). It should be noted that for this analysis, the constant load, $\overline{P}$, will be restricted to cause purely elastic response in the structure, so that the actual stress it causes is equivalent to the fictitious "elastic" stress.

For the remainder of this work and using the translations and adaptations of Koiter, Symonds, and König [3, 4, 19, 20, 32], the following formulation of Melan's lower bound shakedown theorem is adopted: *A solid, Ω (Fig. 2), which is subjected to any cyclic traction F, from the loading domain L, (Fig. 3) on a part $\partial\Omega_F$ of its boundary $\partial\Omega$, will shakedown under this loading domain if one can find any residual stress field, $\boldsymbol{\rho}$, which:*

- *Condition 1 (spatial)* is self-equilibrating, meaning that its divergence over the solid, Ω, is zero and the field satisfies the prescribed traction-free conditions on the solid's boundary, $\partial\Omega_F \cup \Gamma$ (with the normal, $\underline{n}$, Fig. 2) [21]:

$$\begin{aligned} div(\boldsymbol{\rho}) = 0 \quad in \quad \Omega, \\ \boldsymbol{\rho} \cdot \underline{n} = 0 \quad on \quad \partial\Omega_F \cup \Gamma. \end{aligned} \tag{2}$$

- *Condition 2 (pointwise)* is time-independent, meaning that its value at each point does not depend on the applied loading corner, F_i ($\forall i \in [\![1, NC]\!]$), in the loading domain L, (note that $\boldsymbol{\rho}_i$ is the field corresponding to loading corner, F_i):

$$\forall i \in [\![1, NC]\!], \qquad \boldsymbol{\rho}_i = \boldsymbol{\rho}. \tag{3}$$

Fig. 4 Loading domain

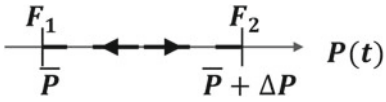

- *Condition 3 (pointwise)* will generate a safe state of stress at each point, $\underline{x}$, in the solid ($\underline{x} \in \Omega$) when it is added to a fictitious "elastic" stress $\sigma_{e,fict}^{F_i}$, associated with any of the loading corners, F_i ($\forall i \in [\![1, NC]\!]$), in the loading domain L. For a yield function, f, and a yield stress, σ_Y, this gives:

$$\forall \underline{x} \in \Omega, \quad \forall i \in [\![1, NC]\!], \qquad f(\boldsymbol{\rho}(\underline{x}) + \sigma_{e,fict}^{F_i}(\underline{x}), \sigma_Y) \leq 0. \tag{4}$$

The conditions have been labeled as pointwise or spatially-dependent (spatial) to highlight differences for use in the following sections. Unlike Conditions 2 and 3 which only have to be satisfied at each point, Condition 1 links all of the points in the solid together through the divergence term and the boundary conditions.

3 Graphical Interpretations of Shakedown Determination with Simplified Elastoplastic Analysis

One approach to finding appropriate residual stress fields for use in Melan's theorem is to use simplified elastoplastic analysis [22–31]. Instead of incrementally following an entire cyclic loading history, a single elastoplastic analysis for one cycle that includes both loading and unloading could be used to calculate a representative residual stress field, $\boldsymbol{\rho}$, developed in a solid, Ω. Then, the residual stress field, $\boldsymbol{\rho}$, is checked so that when it is added to the fictitious "elastic" stresses that would be caused by the same loading process, the sum will remain below the yield level. For more than one cyclic load application (or more than one cyclic load combined with constant loads), the time-independent condition (Eq. 3) is not automatically satisfied. For the following examples, simplified two-corner loading domains (Fig. 4) will be used so that only one path—the one connecting the two corners—has to be analyzed.

In this shakedown determination with a simplified elastoplastic analysis approach, a first step is to compute the residual stress field from loading and unloading the solid, and verify that the self-equilibrating condition is met (Eq. 2). First, the constant load, $\overline{P}$, is applied; this elicits an actual stress which is also the fictitious "elastic" stress (Sect. 2): $\sigma_{actual}^{\overline{P}} = \sigma_{e,fict}^{\overline{P}}$. At this stage, the load applied to the structure is the load corresponding to the first loading corner, $\overline{P} = F_1$. Then, the cyclic load ΔP is applied and the structure is fully loaded (the sum of the constant load, $\overline{P}$ and the extremum value of the cyclic load, ΔP). This corresponds to the second loading corner, F_2. The stress, $\sigma_{actual}^{\overline{P}+\Delta P}$, is now different from the fictitious "elastic" stress, $\sigma_{e,fict}^{\overline{P}+\Delta P}$. This new

fictitious "elastic" stress, $\sigma_{e,fict}^{\overline{P}+\Delta P}$, can be related to the stress caused by the constant load, $\sigma_{e,fict}^{\overline{P}}$ (linearly elastic): $\sigma_{e,fict}^{\overline{P}+\Delta P} = \sigma_{e,fict}^{\overline{P}} + \sigma_{e,fict}^{\Delta P}$.

The residual stress field, $\boldsymbol{\rho}$, is computed by completely unloading the solid: the total fictitious "elastic" stress, $\sigma_{e,fict}^{\overline{P}+\Delta P}$ is subtracted from the total stress, $\sigma_{actual}^{\overline{P}+\Delta P}$:

$$\boldsymbol{\rho} = \sigma_{actual}^{\overline{P}+\Delta P} - \sigma_{e,fict}^{\overline{P}+\Delta P}. \tag{5}$$

The residual stress field, $\boldsymbol{\rho}$, by definition, is automatically self-equilibrating as demonstrated in the following. The stress field, $\sigma_{actual}^{\overline{P}+\Delta P}$, resulting from the applied load $\overline{P} + \Delta P$, satisfies the equilibrium equations (see Fig. 2):

$$\begin{aligned} div\left(\sigma_{actual}^{\overline{P}+\Delta P}\right) &= 0 \quad in\ \Omega \\ \sigma_{actual}^{\overline{P}+\Delta P} \cdot \underline{n} &= \overline{P} + \Delta P \quad on\ \partial\Omega_F \\ \sigma_{actual}^{\overline{P}+\Delta P} \cdot \underline{n} &= 0 \quad on\ \Gamma \end{aligned} \tag{6}$$

The fictitious "elastic" stress field, $\sigma_{e,fict}^{\overline{P}+\Delta P}$, satisfies the same equations, as it is the stress induced by the same loading, $\overline{P} + \Delta P$, but assuming purely elastic behavior:

$$\begin{aligned} div\left(\sigma_{e,fict}^{\overline{P}+\Delta P}\right) &= 0 \quad in\ \Omega \\ \sigma_{e,fict}^{\overline{P}+\Delta P} \cdot \underline{n} &= \overline{P} + \Delta P \quad on\ \partial\Omega_F \\ \sigma_{e,fict}^{\overline{P}+\Delta P} \cdot \underline{n} &= 0 \quad on\ \Gamma \end{aligned} \tag{7}$$

Since the divergence and the scalar product are linear operators, the nullity of the divergence of the residual stress field and the traction-free conditions are ensured by:

$$\begin{aligned} div(\boldsymbol{\rho}) = div\left(\sigma_{actual}^{\overline{P}+\Delta P}\right) - div\left(\sigma_{e,fict}^{\overline{P}+\Delta P}\right) &= 0 \quad in\ \Omega \\ \boldsymbol{\rho} \cdot \underline{n} = \sigma_{actual}^{\overline{P}+\Delta P} \cdot \underline{n} - \sigma_{e,fict}^{\overline{P}+\Delta P} \cdot \underline{n} = \overline{P} + \Delta P &= 0 \quad on\ \partial\Omega_F \\ \boldsymbol{\rho} \cdot \underline{n} = \sigma_{actual}^{\overline{P}+\Delta P} \cdot \underline{n} - \sigma_{e,fict}^{\overline{P}+\Delta P} \cdot \underline{n} &= 0 \quad on\ \Gamma \end{aligned} \tag{8}$$

As the solid, Ω, is elastic-perfectly-plastic, the stress, $\sigma_{actual}^{\overline{P}+\Delta P}$, cannot go beyond the yield limit. One only needs to check that the residual stress field is "safe", meaning that at each point, the residual stress remains below the yield level. In order to illustrate this approach for shakedown determination and gain more insight from a design perspective, a graphical interpretation is presented.

3.1 Example for Combined Cyclic and Constant Loading

Consider a two-component stress state and a von Mises yield function represented as a circle in a S_1, S_2 plane. In this plane, adding and removing stresses can be represented by adding and subtracting vectors; S_1, S_2 are stress components and the plane is not necessarily in principal stress axes. Once the stresses, $\sigma^{F}_{actual}(\underline{x})$, reach the yield limit, they remain at yield on the circle until unloading. For the illustrations presented, only abstract schematic representations are used.

It has been shown above that the residual stress is self-equilibrating. Before considering the following step, a modified stress field, $\tilde{\boldsymbol{\rho}}$, is defined for convenience as the sum of the residual stress field ($\boldsymbol{\rho}$, Eq. 5) with the fictitious "elastic" stress caused by the constant load only, $\sigma^{\overline{P}}_{e,fict}$. This stress is the one remaining in the solid, Ω, after only unloading the cyclic load ΔP:

$$\tilde{\boldsymbol{\rho}} = \boldsymbol{\rho} + \sigma^{\overline{P}}_{e,fict}. \tag{9}$$

The time-independence condition is also automatically satisfied. Once computed, the residual stress ($\boldsymbol{\rho}$, Eq. 5) will not change. Finally, the safe-state condition has only to be checked for the loading corners, at each point, $\underline{x}$, in the solid. For $F_1 = \overline{P}$:

$$\forall\ \underline{x} \in \Omega, \qquad f\left(\boldsymbol{\rho}(\underline{x}) + \sigma^{\overline{P}}_{e,fict}(\underline{x}), \sigma_Y\right) \leq 0 \tag{10}$$

and for $F_2 = \overline{P} + \Delta P$:

$$\forall\ \underline{x} \in \Omega, \qquad f\left(\boldsymbol{\rho}(\underline{x}) + \sigma^{\overline{P}+\Delta P}_{e,fict}(\underline{x}), \sigma_Y\right) = f\left(\sigma^{\overline{P}+\Delta P}_{actual}(\underline{x}), \sigma_Y\right) \leq 0 \tag{11}$$

Equation 11 is automatically satisfied because the solid is elastic-perfectly-plastic. From this point, the safe-state condition must be checked for the modified stress field, $\tilde{\boldsymbol{\rho}}$, (Eq. 9).

For a two-component stress state at a point $\underline{x}$, Fig. 5 illustrates cases where shakedown is and is not possible. If shakedown is not possible at a single point in the structure, shakedown is prevented for the entire structure. In these figures, the *thin solid* lines represent the elastic stresses that result from the applied constant load ($\sigma^{\overline{P}}_{e,fict}\left(\underline{x}\right)$). Following the application of the constant load, an additional cyclic load is then applied and the resulting fictitious "elastic" stresses are shown by the *sparsely-dotted* ($\sigma^{\Delta P}_{e,fict}\left(\underline{x}\right)$). The actual elastoplastic stresses are depicted by *thicker dashed* lines ($\sigma^{F_{a,b}}_{actual}\left(\underline{x}\right)$) and overlap both the *sparsely-dotted* and *thin solid* lines within the elastic domain. The *thick dashed* lines for the actual elastoplastic stresses follow the yield surface (circle) when the yield limit is reached and the load is increased. Upon unloading (elastically), the fictitious "elastic" stress is subtracted from the actual elastoplastic stress ($\sigma^{F_{a,b}}_{actual}\left(\underline{x}\right) - \sigma^{\Delta P}_{e,fict}\left(\underline{x}\right)$). Note that only the cyclic load (and the associated fictitious "elastic" stresses) is removed and the constant load still remains.

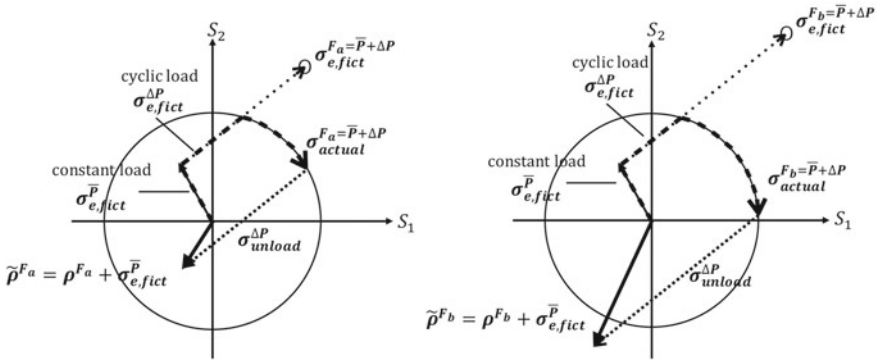

Fig. 5 Schematic illustration of direct method shakedown determination using simplified elasto-plastic analysis. For a two-component stress state at a point ($\underline{x}$), and for a combined cyclic and constant loading case (Fig. 4): shakedown is possible (on the *left*); shakedown is **not** possible (on the *right*)

This process is represented by the *densely-dotted* line ($\sigma^{\Delta P}_{unload}\left(\underline{x}\right)$). The *thick solid* lines show the modified stresses $\tilde{\boldsymbol{\rho}}\left(\underline{x}\right) = \boldsymbol{\rho}\left(\underline{x}\right) + \sigma^{\overline{P}}_{e,fict}\left(\underline{x}\right)$, (Eq. 9). One could argue that although the residual stress found in this way is not necessarily one that allows for shakedown to occur, it could still be possible to find another residual stress that would allow for shakedown. However, the particularity of this approach is that it gives the actual residual stress field that would be caused by the loading and unloading process. If this residual stress field does not allow for shakedown, then the structure will not shakedown. In this versatile approach, a natural ordering of the steps to check the shakedown conditions is suggested by following the physical processes of loading and unloading that the structure experiences. Many other approaches are even more divorced from physical processes and exploit the mathematical freedom in Melan's theorem. Nevertheless, following this process could provide valuable insight for designers regarding how to recover or promote shakedown behavior.

4 Graphical Interpretations of Shakedown Determination with Purely Elastic Analysis

An example of a more mathematical implementation of Melan's theorem uses set theory and can consider the shakedown conditions simultaneously. This kind of approach can also be used to identify new pathways to incorporate shakedown theorems in modern structural topology optimization protocols [45–49]. For the following example, a solid Ω (Fig. 2), and a cyclic loading domain, L, that includes 0 as a loading corner are analyzed (Fig. 3). For ease of understanding, the "pointwise" (time-independence and safe-state) shakedown conditions (Sect. 2) are presented together; the "spatial" (self-equilibrating) condition is applied last.

For each point, $\underline{x}$, in the solid ($\underline{x} \in \Omega$), a feasible stress domain (*for this point*), $f.d.(\underline{x})$, must be found, i.e. all of the stresses $\bar{s}(\underline{x})$ that, for all loading corners F_i ($\forall i \in [\![1, NC]\!]$), satisfy the safe-state condition. The stresses, $\bar{s}(\underline{x})$, are also time-independent because they are load-independent: they do not depend on the loading corner and remain the same for the whole loading domain, L. Note that the new variable, $\bar{s}(\underline{x})$ is defined for convenience to distinguish stresses that only satisfy the pointwise shakedown conditions ($\bar{s}(\underline{x})$) from those that satisfy both the pointwise and spatial shakedown conditions (admissible residual stress fields, $\boldsymbol{\rho}$). Then, for a point in the solid ($\underline{x} \in \Omega$), the feasible stress domain (which will be called a *feasible domain* from now on, $f.d.(\underline{x})$), is composed of the stresses, $\bar{s}(\underline{x})$, satisfying:

$$\forall\, i \in [\![1, NC]\!], \qquad f(\bar{s}(\underline{x}) + \sigma^{F_i}_{e,fict}(\underline{x}), \sigma_Y) \leq 0. \tag{12}$$

For each point, the feasible domain $f.d.(\underline{x})$ can be represented in a stress coordinate system (Fig. 6). Care should be taken to ensure that the same stress coordinate system is used for all of the loading corners. Moreover, the stress coordinate system must also remain the same for the feasible domains at every point in the solid. As a result, the feasible domains, $f.d.(\underline{x})$, are not necessarily determined in principal stress axes as principal stress components depend on the applied loading and they may not be the same for each loading corner and each point in the solid.

With a feasible domain for each point in the solid, combining these domains in space will limit the admissible stress fields. The combination of feasible domains ($f.d.(\underline{x})$) gives a "feasible stress *field* domain" (*for the entire structure*). It is done in a space of dimension (number of stress components) + (number of spatial dimensions): one axis for each stress component and one axis for each spatial direction. In this space, the feasible domain for each point ($\underline{x}$), is drawn at the spatial coordinates of the point in the solid and extends along stress component axes (Fig. 7).

To meet both the pointwise and spatial conditions (Eqs. 2–4, Sect. 2), an admissible stress field, $\boldsymbol{\rho}$, is found in the intersection of the self-equilibrating stress fields and the feasible stress field domain. Thus, the representation of an admissible stress field, $\boldsymbol{\rho}$, in the space of dimension (number of stress components) + (number of spatial dimensions) must remain within the boundaries set by the variation of feasible domains in the solid (i.e. the feasible stress field domain) (see schematic in Fig. 7). For ease of visualization, only the satisfaction of the divergence equation is shown; additional boundary conditions would further limit the admissible fields, $\boldsymbol{\rho}$, within

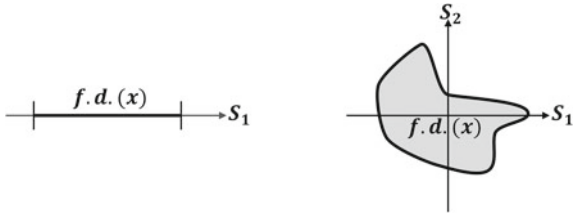

Fig. 6 Schematic of a feasible domain for a point, $f.d.(\underline{x})$, with feasible stress values. *Left* example for a single stress component. *Right* example for a two-component stress

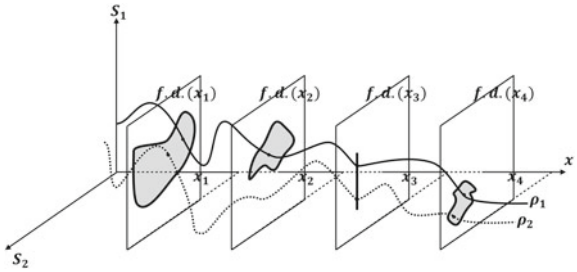

Fig. 7 Schematic illustration of the variation of feasible domains at various points in a structure. Each feasible domain, $f.d.(\underline{x})$, is drawn at the spatial coordinates of the point in the structure and extends along stress component axes (S_1, S_2). The representation of an admissible stress field, $\boldsymbol{\rho}$, in the space of dimension (number of stress components) + (number of spatial dimensions) must remain within the boundaries set by the variation of feasible domains in the solid (i.e. the feasible stress **field** domain). Two possibilities for $\boldsymbol{\rho}$ are given: the example with the *solid line* ($\boldsymbol{\rho}_1$) belongs to the feasible stress field domain whereas the example with the *dotted line* ($\boldsymbol{\rho}_2$) does not

the feasible stress field domain. This "intersection of domains" approach is useful for both understanding and designing to shakedown. Modifications of the material, geometric, and problem parameters will change these two domains: reducing, enlarging, translating them and affecting the size and existence of the intersection zone in which the admissible residual stress fields, $\boldsymbol{\rho}$, reside.

4.1 Example for only Cyclic Loading

To schematically illustrate this kind of implementation of Melan's theorem, a four-corner cyclic loading domain, L (Fig. 3), is used. The simplified example assumes a linear yield function, f, and a one-dimensional structure, Ω, that experiences a single-component stress. To represent this problem in a continuous way, one would have to consider the pointwise shakedown conditions (Eqs. 3 and 4) at each point in the solid. In this example, only three points (x_1, x_2, x_3) are analyzed. The fictitious "elastic" stresses caused by the loading corner (F_1, F_2, F_3, or $F_4 = 0$), for these points in the structure are $\sigma^{F_i}_{e,fict}(x_1)$, $\sigma^{F_i}_{e,fict}(x_2)$, and $\sigma^{F_i}_{e,fict}(x_3)$.

A schematic case where shakedown is possible is illustrated. The feasible domains, $f.d.(\underline{x})$, at each point in the solid ($\underline{x} \in \Omega$) must be computed (Figs. 8, 9 and 10). These computations rely on analytical elasticity solutions or on approximations using finite element analysis. For the examples below, only abstract schematics are presented. The safe-state condition has to be satisfied for all four loading corners ($F_1, F_2, F_3, F_4 = 0$). The feasible domain for the points analyzed in the structure (x_1, x_2, x_3) is determined when the sum of the fictitious "elastic" stresses, $\sigma^{F_1}_{e,fict}\, \sigma^{F_2}_{e,fict}\, \sigma^{F_3}_{e,fict}\, \sigma^{F_4}_{e,fict}$ and $\bar{s}(\underline{x})$ (Eq. 12) remain elastic.

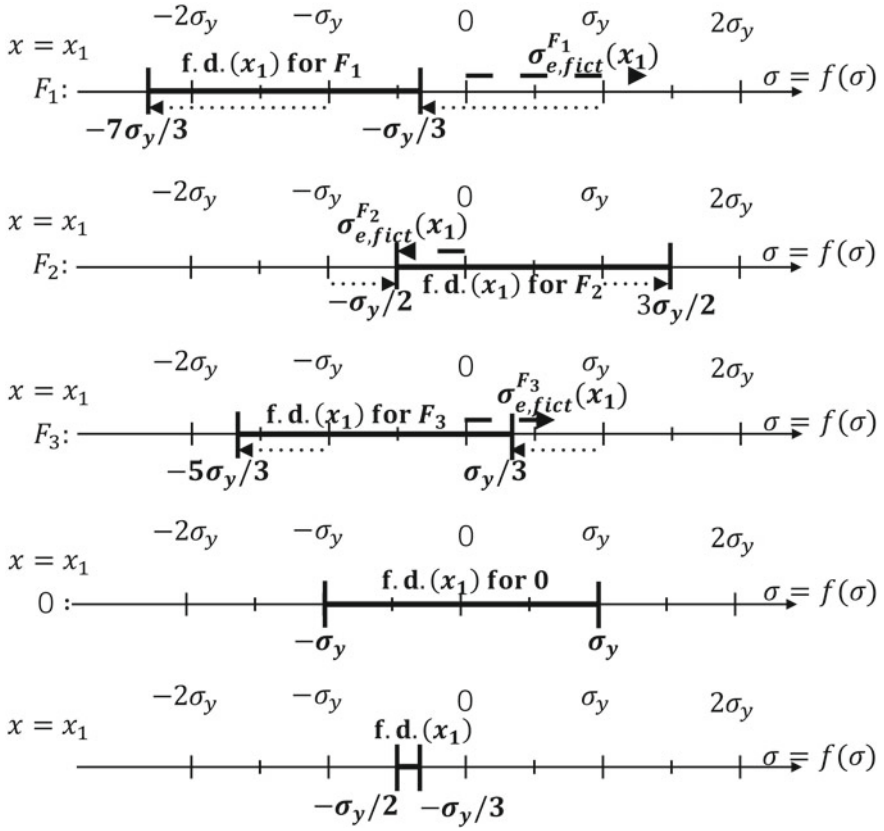

Fig. 8 Feasible domain (f.d.) for point x_1

Within each of the Figs. 8, 9 and 10 (and for each corresponding point x_1, x_2, x_3), there are several linear plots: one indicating the feasible domain for each of the loading corners (F_1, F_2, F_3, $F_4 = 0$) and a final plot that shows the feasible domain for the point (x_1, x_2 or x_3), which is the intersection of all of the feasible domains for each of the loading corners. The fictitious "elastic" stresses are computed for each loading corner and are represented by *dashed vectors* along linear stress continuums. These plots also illustrate the yielding limits (using a von Mises function $f(\sigma) = \sigma$) in tension ($\sigma = \sigma_Y$) and compression ($\sigma = -\sigma_Y$). The feasible domain ($f.d.(\underline{x})$ for F_i) is represented by *thick black lines*. This domain is the translation of the elastic domain ($[-\sigma_Y, \sigma_Y]$) by the fictitious elastic stress ($-\sigma_{e,fict}^{F_i}(\underline{x})$), i.e. in the opposite direction and with the same magnitude. This translation is shown by the *dotted lines* at the boundaries of the elastic domain. Note that for the loading corner $F_4 = 0$, (no external loading), there are no associated fictitious elastic stresses and the translated elastic domain is the original elastic domain.

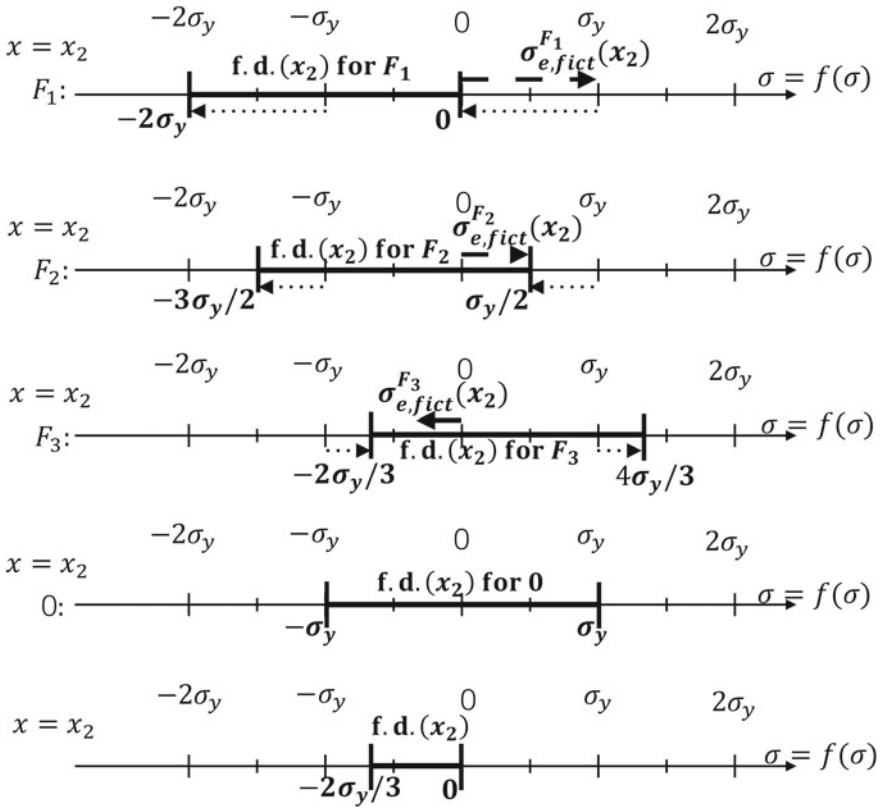

Fig. 9 Feasible domain (f.d.) for point x_2

Combining the final feasible domains in space for each point in the structure ($\underline{x} \in \Omega$)—for example, placing them side by side along a spatial axis, allows one to visualize the limitations on the feasible stress field domain (Fig. 11). For the example presented here, it is assumed that, for points between those considered, the limits of their feasible domains will also fall linearly between the determined limits. For more general problems, finite element approximations and mesh sensitivity studies are needed. With Fig. 11, the self-equilibrating condition can be applied to find the admissible stress field, $\boldsymbol{\rho}$, (i.e. enforcing the nullity of the divergence and the traction-free state on the part of the boundary $\partial\Omega_F \cup \Gamma$):

$$div(\boldsymbol{\rho}) = \frac{\partial \boldsymbol{\rho}(x)}{\partial x} = 0 \quad in\,\Omega, \quad \Rightarrow\ \boldsymbol{\rho} = constant \quad in\,\Omega. \tag{13}$$

For this example, the divergence equation requires one to find a constant function, $\boldsymbol{\rho}$, which, for each point of the solid ($\underline{x} \in \Omega$), would remain in the feasible domain:

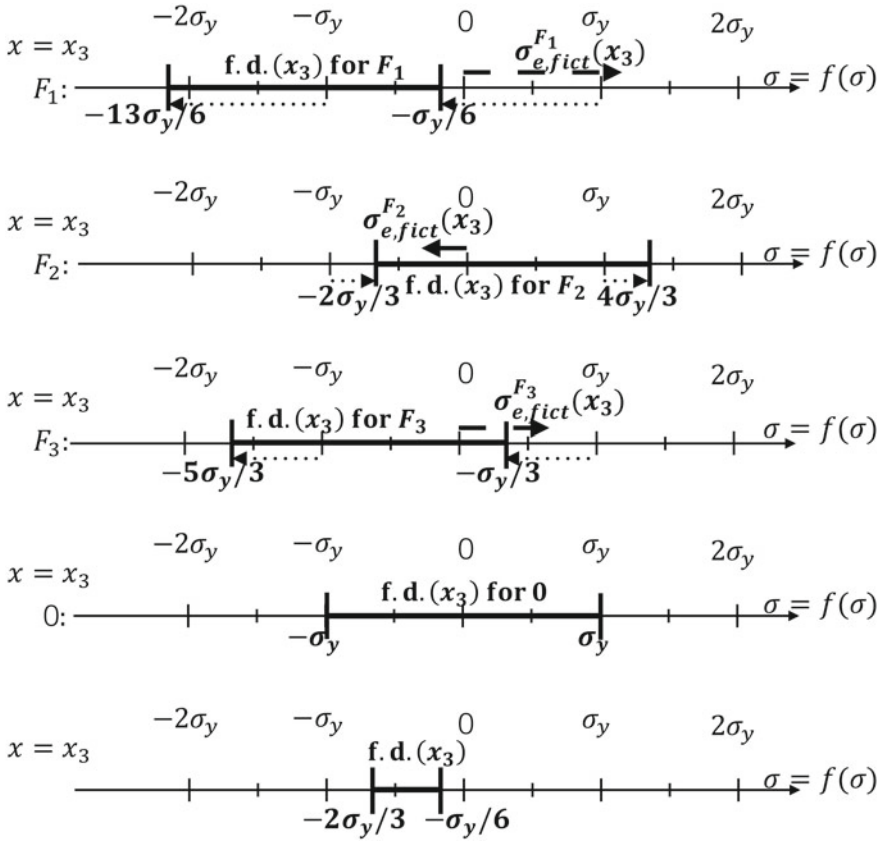

Fig. 10 Feasible domain (f.d.) for point x_3

$$\exists \boldsymbol{\rho} \in \mathbb{R} \quad s.t. \quad \forall \underline{x} \in \Omega, \qquad \boldsymbol{\rho}(\underline{x}) = \boldsymbol{\rho} \in f.d.(\underline{x}), \tag{14}$$

The self-equilibrating shakedown condition (Eq. 2) does not always require a constant residual stress field $\boldsymbol{\rho}$ (Fig. 7).

Figure 11 shows that, for this schematic example, one can find some shakedown solutions (on the left, in the middle). In this way one assures that the whole structure, Ω, will shakedown under the applied loading domain, L. In contrast, one can imagine an alternative scenario for which there is no constant function (i) that will satisfy the self-equilibrating condition and (ii) that is also a member of the feasible stress field domain; thus shakedown is not possible (Fig. 11, on the right).

This example highlights several factors that could prevent shakedown for a structure; these factors present design opportunities to recover shakedown behavior. An empty feasible domain for a single point in the structure will prevent shakedown for the entire structure (the feasible domain for point x_1 in Figs. 8 and 9 could have been

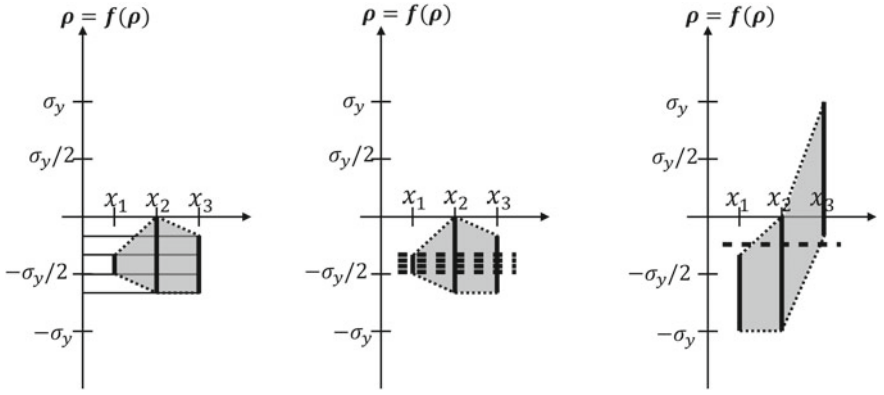

Fig. 11 *Left* feasible stress field domain from the combination of each point's feasible domain. *Middle* the same feasible stress field domain is shown with the self-equilibrating condition that indicates shakedown is possible. *Right* example of a possible feasible stress field domain where the intersection with the self-equilibrating fields is empty and shakedown is not possible

empty and then shakedown would not be possible for the structure). The feasible domain *for a point* may be empty due to the magnitude of stress levels associated with a single loading corner (i.e. greater than $2\sigma_Y$ in this example), or because the combination of feasible domains for each loading corner yields an empty set when combined for the final feasible domain determination at a point. Shakedown may also be prevented due to an empty feasible stress *field* domain. This failure relates to the "spatial" self-equilibrating shakedown condition: in these examples, the condition requires one to find a constant function that would remain in the feasible domain for every point in the solid (Fig. 11). As a lower bound for a structure, if it is found that shakedown is not possible for a loading corner within a given loading domain, L, then shakedown is also not possible for the entire loading domain.

For this kind of implementation of Melan's theorem, an example has been given to illustrate the set theory approach. It is a search for the intersection of stress fields that are admissible from pointwise and spatial-condition perspectives. It should be again emphasized that this kind of implementation does not require any elastoplastic analysis, it is based purely on elastic solutions. However, it will not provide information about the residual stress state, $\boldsymbol{\rho}$, that actually exists in the solid. Indeed, the uniqueness of the residual stress field is derived from the load history [19] which is not considered in direct methods.

5 Discussion

The graphical interpretations and approaches presented for some implementations of Melan's Lower Bound Shakedown Theorem offer tools for deeper understanding and for making design choices. The mathematical processes used in methods for shake-

down determination are often buried in computational codes. However, as is the case with many graphical representations in 2D and 3D, their practical utility is limited and the graphical tools presented are not intended to replace other tools nor are they recommended for complex geometries or loading domains. Nevertheless, the graphical tools offer complementary information to traditional Bree Interaction Diagrams. Bree diagrams give bounds for elastoplastic responses (including shakedown) under prescribed loading combinations but they do not indicate how shakedown conditions are met. By elucidating how pointwise and spatial shakedown conditions are met, directions for promoting and recovering shakedown behavior that are not indicated in the Bree Diagrams may be highlighted. These may include modifications of the material, geometry, and boundary conditions. Even for obvious changes such as increasing the material yield strength, interaction diagrams will give the revised shakedown domain, but the graphical approach and interpretations presented here allow one to see how and why this parameter influences the shakedown domain from a lower-bound perspective.

In the previous examples, several simplifying assumptions were made such as ignoring the dependence of material properties (yield strength σ_Y, Young's Modulus E), on parameters such as temperature [33]. Including these effects would fall under the pointwise conditions, modifying the shape of the feasible domain for each point. In addition, in the analysis presented, only simple tractions on the boundary, cycling between 0 and a maximum load have been considered. Including other loads, such as volumetric loads or temperature gradients is possible but adds significant visual complexity. The dimensions required to draw the feasible domains and especially the combination of feasible domains for many structures are often too high for visualization and defeat the purpose of these tools for understanding. Nevertheless, revisiting this well-established theorem from a graphical and pedagogical approach, provides a foundation for new interdisciplinary applications, including identifying pathways for incorporation of shakedown in modern structural topology optimization schemes.

6 Conclusion

Several graphical interpretations of direct methods that implement Melan's lower bound shakedown theorem have been developed. They serve as educational and simple design tools to complement existing Bree Interaction Diagrams. Where Bree Diagrams give the domains of expected elastoplastic responses for a structure under prescribed loading conditions, the graphical approaches developed here show how and why shakedown conditions are met. They provide a graphical representation of the mathematical processes at the foundation of computational shakedown codes. They also provide design insight by highlighting directions for promoting or recovering shakedown behavior in structures.

Acknowledgements Dr. Vermaak would like to acknowledge that, in part, this material is based upon work supported by the Air Force Office of Scientific Research under award number FA9550-16-1-0438. The authors would also like to thank Dr. Hany Fayek Abdalla for helpful discussions about the technique in Abdalla et al. [22].

References

1. Grüning M (1926) Die Tragfähigkeit statisch unbestimmter Tragwerke aus Stahl bei beliebig häufig wiederholter Belastung. Springer
2. Bleich H (1932) Über die Bemessung statisch unbestimmter Stahltragwerke unter Berücksichtigung des elastisch-plastischen Verhaltens des Baustoffes. Bauingenieur 19(20):261–266
3. Melan E (1938) Der Spannungszustand eines Mises-Henckyschen Kontinuums bei veraenderlicker Belastung. Sitzber Akad Wiss 147:73–78
4. Melan E (1938) Zur Plastizität des räumlicken Kontinuums. Ing Arch 8:116–126
5. Weichert D, Ponter A (2014) A historical view on shakedown theory. In: The History of theoretical, material and computational mechanics-mathematics meets mechanics and engineering. Springer, pp 169–193
6. Simoens B, Lefebvre M, Nickell R, Minami F (2012) Experimental demonstration of shakedown in a vessel submitted to impulsive loading. J Press Vessel Technol 134:1–6
7. Ponter A, Hearle A, Johnson K (1985) Application of the kinematical shakedown theorem to rolling and sliding point contacts. J Mech Phys Solids 33(4):339–362
8. Begley MR, Evans AG (2001) Progressive cracking of a multilayer system upon thermal cycling. J Appl Mech 68(4):513–520
9. Tao M, Mohammad LN, Nazzal MD, Zhang Z, Wu Z (2010) Application of shakedown theory in characterizing traditional and recycled pavement base materials. J Transp Eng 136(3):214–222
10. García-Rojo R, Herrmann HJ (2005) Shakedown of unbound granular material. Granular Matter 7(2–3):109–118
11. Sun H, Pathak A, Luntz J, Brei D, Alexander PW, Johnson NL (2008) Stabilizing shape memory alloy actuator performance through cyclic shakedown: An empirical study. In: The 15th international symposium on: smart structures and materials and nondestructive evaluation and health monitoring. International Society for Optics and Photonics, p 69300
12. Peigney M (2014) On shakedown of shape memory alloys structures. Ann Solid Struct Mech 6(1–2):17–28
13. Reedlunn B, Daly S, Shaw J (2013) Superelastic shape memory alloy cables: part II–subcomponent isothermal responses. Int J Solids Struct 50(20–21):3027–3044
14. Bree J (1967) Elastic-plastic behaviour of thin tubes subjected to internal pressure and intermittent high-heat fluxes with application to fast-nuclear-reactor fuel elements. J Strain Anal Eng Des 2(3):226–238
15. ASME Boiler and Pressure Vessel Code (2003) ASME, New York
16. BS 5500: British standard specification for fusion welded pressure vessels (1996) British Standards Institute, London
17. R5 Assessment procedure for the high temperature response of structures (1990) Nuclear Electric PLC
18. Abdel-Karim M, Ohno N (2000) Kinematic hardening model suitable for ratchetting with steady-state. Int J Plast 16(3–4):225–240
19. Koiter WT (1960) General theorems for elastic-plastic solids. North-Holland Amsterdam
20. König J (1987) Shakedown of elastic-plastic structures. Elsevier, The Netherlands
21. Bower A (2009) Applied mechanics of solids. CRC Press
22. Abdalla HF, Megahed MM, Younan MYA (2007) A simplified technique for shakedown limit load determination. Nucl Eng Des 237:1231–1240

23. Abdalla HF, Megahed MM, Younan MYA (2009) Comparison of pipe bend ratchetting/shakedown test results with the shakedown boundary determined via a simplified technique. In: Proceedings of the ASME 2009 pressure vessels and piping division conference PVP2009, pp 659–666
24. Abdalla HF, Younan MYA, Megahed MM (2011) Shakedown limit load determination for a kinematically hardening 90° pipe bend subjected to steady internal pressures and cyclic bending moments. J Press Vessel Technol 133:051212–1–10
25. Korba A, Megahed MM, Abdalla HF, Nassar MM (2013) Shakedown analysis of 90-degree mitred pipe bends. Eur J Mech-A/Solids 40:158–165
26. Elsaadany MS, Younan MY, Abdalla HF (2014) Determination of shakedown boundary and failure-assessment-diagrams of cracked pipe bends. J Press Vessel Technol 136(1):011209
27. Abdalla HF (2014) Elastic shakedown boundary determination of a cylindrical vessel-nozzle intersection subjected to steady internal pressures and cyclic out-of-plane bending moments. Nucl Eng Des 267:189–196
28. Oda AA, Megahed MM, Abdalla HF (2015) Effect of local wall thinning on shakedown regimes of pressurized elbows subjected to cyclic in-plane and out-of-plane bending. Int J Press Vessels Pip 134:11–24
29. Abdalla HF (2014) Shakedown limit load determination of a cylindrical vessel-nozzle intersection subjected to steady internal pressures and cyclic in-plane bending moments. J Press Vessel Technol 136(5):051602
30. Abdalla HF (2014) Shakedown boundary determination of a 90° back-to-back pipe bend subjected to steady internal pressures and cyclic in-plane bending moments. Int J Press Vessels Pip 116:1–9
31. Hafiz YA, Younan MY, Abdalla HF (2015) A proposal for a simplified assessment procedure to api-579 standard. J Press Vessel Technol 137(3):031007
32. Symonds PS (1951) Shakedown in continuous media. J Appl Mech-Trans ASME 18(1):85–89
33. Peigney M (2014) Shakedown of elastic-perfectly plastic materials with temperature-dependent elastic moduli. J Mech Phys Solids 71:112–131
34. Weichert D (1984) Shakedown at finite displacements; a note on Melan's theorem. Mech Res Commun 11(2):121–127
35. Spiliopoulos KV (1997) On the automation of the force method in the optimal plastic design of frames. Comput Methods Appl Mech Eng 141(1):141–156
36. Maier G (1969) Shakedown theory in perfect elastoplasticity with associated and nonassociated flow-laws: a finite element, linear programming approach. Meccanica 4(3):250–260
37. Bodovillé G, de Saxcé G (2001) Plasticity with non-linear kinematic hardening: modelling and shakedown analysis by the bipotential approach. Eur J Mech-A/Solids 20(1):99–112
38. Garcea G, Leonetti L (2013) Decomposition methods and strain driven algorithms for limit and shakedown analysis. In: Limit state of materials and structures. Springer, pp 19–43
39. Ponter AR, Engelhardt M (2000) Shakedown limits for a general yield condition: implementation and application for a von mises yield condition. Eur J Mech-A/Solids 19(3):423–445
40. Ponter A, Chen H (2001) A minimum theorem for cyclic load in excess of shakedown, with application to the evaluation of a ratchet limit. Eur J Mech-A/Solids 20:539–553
41. Stein E, Zhang G, König JA (1992) Shakedown with nonlinear strain-hardening including structural computation using finite element method. Int J Plast 8(1):1–31
42. Vu D, Staat M, Tran I (2007) Analysis of pressure equipment by application of the primal-dual theory of shakedown. Commun Numer Methods Eng 23:213–225
43. Simon JW, Weichert D (2013) Interior-point method for lower bound shakedown analysis of von Mises-type materials. In: Limit state of materials and structures. Springer, pp 103–128
44. Wiechmann K, Stein E (2006) Shape optimization for elasto-plastic deformation under shakedown conditions. Int J Solids Struct 43(22):7145–7165
45. Allaire G, Jouve F, Toader AM (2004) Structural optimization using sensitivity analysis and a level-set method. J Comput Phys 194(1):363–393
46. Wang M, Wang X, Guo D (2003) A level set method for structural topology optimization. Comput Methods Appl Mech Eng 192(1):227–246

47. Bendsoe M, Sigmund O (2004) Topology optimization: theory, methods and applications. Springer
48. Kammoun Z, Smaoui H (2015) A direct method formulation for topology plastic design of continua. In: Direct Methods for Limit and Shakedown Analysis of Structures. Springer, pp 47–63
49. Kammoun Z, Smaoui H (2014) A direct approach for continuous topology optimization subject to admissible loading. Comptes Rendus Mécanique 342(9):520–531